# Fabrication of highly hydrophobic two-component thermosetting polyurethane surfaces with silica nanoparticles

[1]*Guang Yang,* [1]*Jialu Song,* [2]*Xianghui Hou*

[1]Key Laboratory of Aerospace Materials and Performance (Ministry of Education), School of Materials Science and Engineering, Beihang University, Beijing 100191, China

[2]Faculty of Engineering, University of Nottingham, University Park, Nottingham NG7 2RD, UK

Corresponding Author: Guang Yang*

*E-mail: yangguang@buaa.edu.cn

## Abstract

Highly hydrophobic thermosetting polyurethane (TSU) surfaces with micro-nano hierarchical structures were developed by a simple process combined with sandpaper templates and nano-silica embellishment. Sandpapers with grit sizes varying from 240 to 7000 grit were used to obtain micro-scale roughness on an intrinsic hydrophilic TSU surface. The surface wettability was investigated by contact angle measurement. It was found that the largest contact angle of the TSU surface without nanoparticles at 102 ± 3 ° was obtained when the template was 240-grit sandpaper and the molding progress started after 45 min curing of TSU. Silica nanoparticles modified with polydimethylsiloxane were scattered onto the surfaces of both the polymer and the template to construct the desirable nanostructures. The influences of the morphology, surface composition and the silica content on the TSU surface wettability were studied by scanning electron microscopy (SEM), attenuated total reflection (ATR) infrared (IR) spectroscopy, X-ray photoelectron spectroscopy (XPS) and contact angle measurements. The surface of the TSU/$SiO_2$ nanocomposites containing 4 wt% silica

nanoparticles exhibited a distinctive dual-scale structure and excellent hydrophobicity with the contact angle above 150°. The mechanism of wettability was also discussed by Wenzel model and Cassie-Baxter model.

**Keywords:** Thermosetting polyurethane; Hydrophobicity; Sandpaper template; Silica nanoparticles; Hierarchical structure.

## 1 Introduction

According to the diverse monomers and formulation selections, polyurethane (PU) is of versatile nature and has many unique properties, including good weather and abrasion resistance, excellent mechanical behavior, high elasticity, and low temperature flexibility [1]. These properties make PU widely used in forms of foams, elastomers, fibers, adhesives, leather, and coatings [2-9], etc. Generally, PU can be classified into thermoplastic polyurethane (TPU) and thermosetting polyurethane (TSU) on the basis of the molecular chain structure. Particularly, TSU consists of the complex chemical crosslinking network. This relates to the good thermal stability, high strength and excellent dimensional stability of TSU resin, which also made it possible to be used as the surface and coating materials in aerospace, automotive, construction and medical equipment [10.11], etc. However, most of common TSU surfaces show moderate hydrophilicity owing to the polar groups and interaction with water droplets, which hampers their practical application in terms of water resistance.

Up to now, the fabrication of hydrophobic PU surfaces has mainly focused on chemical and physical modification [12-14]. For instance, Wu et al. [12] introduced polydimethylsiloxane (PDMS) into the PU chain and obtained superhydrophobic surfaces due to the enrichment of PDMS at the air-solid interface and the prepared rough structure. Steele et al. [13] fabricated moisture-cured polyurethane (MCPU)/organoclay compound coatings with the contact angle over 160°. In their study,

MCPU was modified by waterborne perfluoroalkyl methacrylic copolymer and organoclay was further decorated with fatty amine/amino-silane. Tang et al. [14] achieved superhydrophobic TPU/$MoS_2$ nanocomposite coatings via spraying $MoS_2$ nanoparticles onto the TPU surfaces and subsequently modifying with 1H, 1H, 2H, 2H-perfluorooctyltrichlorosilane (PFOT), which were applied to reduce the surface energy.

Template method has been used to effectively control the morphology and patterns of the surface by altering the nature and geometrical microstructure of templates, including hard and soft template method. Hard templates mainly involve porous anodic aluminum oxide [15], metal monomer [16], silica [17], and carbon fibers [18], etc. Soft templates are normally related to polymers, such as PDMS [19] and polystyrene (PS) [20], etc. Due to the simplicity and the possibility for large-area products, the template method has a great potential in fabricating desirable rough microstructure on polymer surfaces. Zhao et al. [21] prepared a superhydrophobic TPU film by dip coating a porous anodic alumina template using a TPU solution. The water contact angle of the rough TPU surface is up to 152°, contributed from the enhanced roughness created by the template.

Nanoparticles have been frequently utilized to enhance the surface properties because of their flexible sizes and adjustable wettability. Among them, nano-sized silica is a popular candidate for modifying materials with the advantages of large specific surface area, small particle size, good mechanical and thermal stability, and commercial availability [22-24]. Silica nanoparticles with hydrophobic modification are entensively investigated because they are applicable to build micro-nano structures with micro-scale particles or micro-structured polymer and can effectively change hydrophilic surfaces to durable hydrophobic surfaces with rapid and simple fabrication processes, which is particularly important for the hydrophilic polymer surfaces with excellent comprensive

performances. Wu et al. [25] fabricated a superhydrophobic surfaces with micro-nano structures via simply spraying water polyurethane dispersions with hydroxyl-silicone-oil modified microscale tourmaline particles and the nano-scale silica particles. Wong et al. [26] reported a synthesis of an ultra-durable and storage-stable superhydrophobic surface by sequentially spraying of a novel polyurethane-acrylic colloidal suspension and a hydrophobic fluoro-silica nanoparticle solution. Seyfi et al. [27] created a robust and thermally stable superhydrophobic TPU surface via spin coating silica nanoparticles dispersion. The weight ratio of the TPU to silica nanoparticles was 1:1. In another study, they enhanced the hydrophobicity of thermoplastic PU surfaces and fabricated micro-nano dual structures through a phase separation technique by mixing ethanol and silica nanoparticles [28]. Ferrari's group prepared a superhydrophobic organic-inorganic coating by simply mixing fluoropolymer blend and fumed silica nanoparticles and then rapidly spraying onto glass or metal substrates, which contributed to the application of the superhydrophoic coatings in seawater [29-31].

In this study, different types of sandpaper templates and nano-silica particles were conjointly used to fabricate hydrophobic TSU surfaces with unique micro-nano dual structures. There was no need to modify TSU itself, and the nano-silica particles were only added on the top layer of the surface, which efficiently simplified the fabrication process and saved nano-silica partilces. The optimum technological conditions including the starting time of molding process, the type of sandpapers, the silica content and the molding pressure were determined from the surface wettability. The morphology and composition of the PU surfaces were investigated by scanning electron microscopy (SEM), attenuated total reflection (ATR) infrared (IR) spectroscopy and X-ray photoelectron spectroscopy (XPS).

## 2 Experimental sections

88 2.1 Materials

89 Two-component thermosetting polyurethane (Vytaflex@40) was purchased from Smooth-On Inc.,
90 USA. Hydrophobic silica nanoparticles modified by PDMS (Aerosil R202) was obtained from Evonik
91 Industries, Germany. Its specific surface area is 100 ± 20 $m^2$/g and the primary particle size is 14 nm.
92 Sandpapers with the abrasive particles of silicon carbide were supplied by Shanghai Shenming
93 Abrasives Co. Ltd., China and the grit size ranged from 7000-grit to 240-grit.

94 2.2 Preparation of rough PU surfaces

95 PU surfaces with micro-scale structures were constructed via the template method. Part A and B
96 of PU (1 g) were mixed at a base/cross-linker ratio of 1:0.85, and subsequently dip-coated on glass
97 slide surface (3 × 3 $cm^2$). After curing a period of time at room temperature, the sandpaper templates
98 were put onto the PU samples with a certain pressure, respectively. The starting time of the molding
99 process varied from 0 to 60 min after curing PU. Then, the PU layers were further cured for 24 h at
100 room temperature. After that, the templates were peeled off immediately. The samples were named as
101 shown in Table 1 and Table 2, respectively. For comparison purposes, smooth surface samples were
102 also prepared using the same curing conditions.

103 **Table 1** Nomenclature used for the rough PU surfaces produced using sandpaper templates.

| Sample | PU-1 | PU-2 | PU-3 | PU-4 | PU-5 | PU-6 | PU-7 | PU-8 | PU-9 |
|---|---|---|---|---|---|---|---|---|---|
| Grit number | 240 | 1000 | 1200 | 1500 | 2000 | 2500 | 3000 | 5000 | 7000 |

104 **Table 2** Nomenclature used for the samples with different starting time of the molding progress.

| Sample | PU0 | PU15 | PU30 | PU45 | PU60 |
|---|---|---|---|---|---|
| Starting time | 0 | 15 | 30 | 45 | 60 |

105 2.3 Preparation of PU/$SiO_2$ nanocomposite surfaces

106 Template method and surface modification were synchronously used to fabricate hydrophobic PU
107 surfaces. The fumed silica particles were dehydrated in the oven at 105°C for 2 h before use. Part A
108 and B of PU ($W_0$) were also mixed at a ratio of 1:0.85, and subsequently dip-coated on glass slide
109 surface ($3 \times 3$ $cm^2$). Specific amount of silica nanoparticles ($W_1$) were uniformly scattered onto the
110 surfaces of both a selected sandpaper template and uncured PU. The nanoparticles that were not bonded
111 to the sandpaper surface were gently shaken off and recycled. The nano-silica particles were well
112 distributed over the entire surface without severe aggregation. A very thin layer of nano-silica particles
113 ($W_2$) remained on the templates by the weak adsorption between the sandpaper surface and
114 nanoparticles. After curing 45 min at room temperature, the sandpaper templates covered with silica
115 nanoparticles were then placed upon the PU/$SiO_2$ surfaces with a certain pressure, varying from 3 to 8
116 MPa, respectively. The nanocomposites were also further cured for 24 h at room temperature and then
117 the templates were peeled off. A very small amount of nanoparticles still remained on the sandpapers.
118 Similarly, the unbonded nanoparticles on the cured PU rough surfaces were also gently shaken off and
119 recycled. The rest of nano-silica particles ($W_3$) remained decorating the rough PU surfaces. The result
120 PU/$SiO_2$ nanocomposite samples ($W_4$) were named as shown in Table 3. Figure 1 shows a generic route
121 used for preparing all nanocomposites studied in this work. For comparison purposes, PU/$SiO_2$
122 nanocomposite samples without templates were also prepared using the same curing conditions.

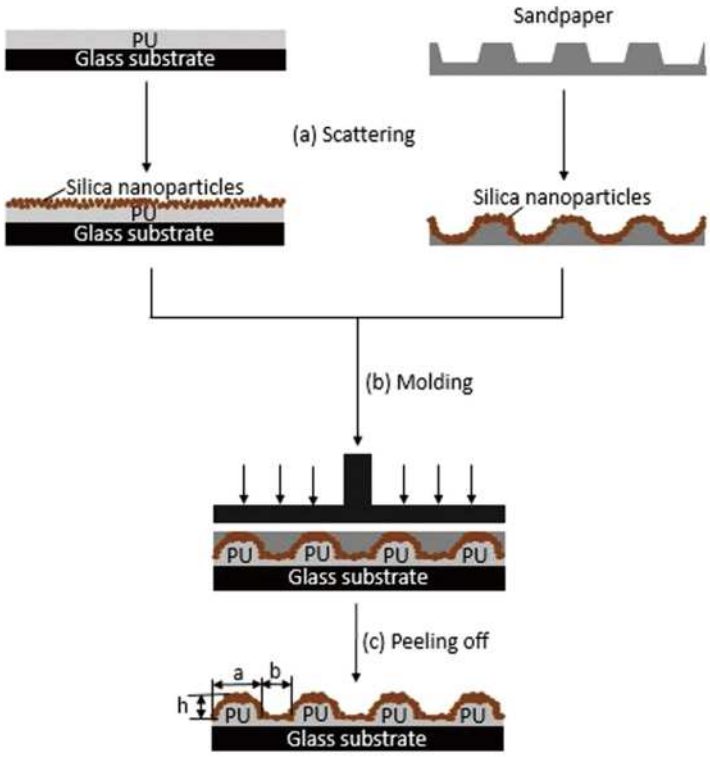


**Fig. 1.** Schematic representation of the preparation process for the fabrication of PU/$SiO_2$ nanocomposite surfaces with the rough structures made of pillars with inclined side walls.

2.4 Characterization

Water contact angles were measured by the sessile drop method on an optical contact angle meter (OCA 20, Dataphysics Co., Germany) at ambient temperature. The volume of the individual deionized water droplet was 4μL. The reported contact angle value was the average of five separate measurements at different locations on the same sample. The surface morphology was observed by scanning electron microscopy (SEM, Hitachi SU8010, Japan) at an activation voltage of 20 kV. All the samples were vacuum-coated with gold. 3D images and geometric parameters of the surface were captured by a digital microscope (Hirox KH-7700, Japan). Each of the presented geometric parameters was the average of 10 measurements at different locations on the same rough surface. The surface compositions and the silica nanoparticle contents of the top layer on the PU/$SiO_2$ nanocomposite

surfaces were characterized and calculated, respectively, by ATR-IR and XPS. ATR-IR studies were carried out by a FTIR spectrometer (Nicolet 6700, Thermo Fisher, USA). The internal reflection prism was ZnSe and the incident angle was 45 °, respectively. XPS data was collected by an photoelectron spectroscopy analyzer (Thermo ESCALAB 250XI, USA) equipped with a Al Kα (hυ = 1486.6 eV) X-ray source, which was operated at 150 W and $1\times10^{-7}$ Pa vacuum degree. The maximum information depth of the XPS study was not more than 10 nm. The storage-stability of the nanocomposite samples was examined after storing in air for three months. The stability of the surfaces under shear force and impact force conditions was also verified. Both ends of the nanocomposite samples without the glass substrates were clamped with fixtures and twisted 180° ten times a day. After torsion, the samples were placed upright and sprayed water vertically. The distance between the sprater and the sample was 20 cm and the quantity was 10 ml, once a day. The contact angles of the surfaces was tested after 10, 30, 60 and 90 days.

The content of nano-silica particles on the PU/$SiO_2$ composites in the Table 3 were calculated using the following formula,

$$SiO_2 \text{ content (wt\%)} = (W_4 - W_0)/W_4 \quad (1)$$

**Table 3** Nomenclature used for the nanocomposite samples with different $SiO_2$ weight content.

| Sample | PU-Si1.5 | PU-Si2 | PU-Si3 | PU-Si3.5 | PU-Si4 | PU-Si5 | PU-Si6 |
|---|---|---|---|---|---|---|---|
| PU added ($W_0$, mg) | 1000 | 1000 | 1000 | 1000 | 1000 | 1000 | 1000 |
| $SiO_2$ added ($W_1$, mg) | 30 | 50 | 55 | 68 | 76 | 85 | 100 |
| $SiO_2$ left ($W_3$, mg) | 14.5-15.5 | 20-21 | 30-31 | 36-37 | 40.5-42 | 51.5-53 | 63-64 |
| $SiO_2$ content (wt %) | 1.4-1.5 | 2.0-2.1 | 2.9-3.0 | 3.5-3.6 | 3.9-4.0 | 4.9-5.0 | 5.9-6.0 |

## 3. Results and discussion

### 3.1 Technical factors of the templating process

As mentioned above, sandpaper template method has been developed to produce hydrophobic surfaces. In this study, micro-scaled structures were created using the sandpaper templates. During the molding process, both the starting time of templating and the types of sandpapers had significant effects on the wettability of PU surfaces.

The water contact angle results of PU surfaces fabricated with different starting time are shown in Table 4. 240-grit sandpaper and the pressure of 5 MPa were used in this attempt. The starting time was calculated as the curing time of PU at the point of templating. Due to its strongly polar functional groups in the molecular chain, the smooth cured PU surface exhibited a rather hydrophilic behavior with a contact angle of 67 ± 2°. With the delay of the starting time, the water contact angles on rough PU surfaces increased firstly and then decreased. The samples prepared within 30 min curing PU were quite difficult to be peeled off, because the short curing time led to the low curing degree, which contributed to the stronger adhesion between PU and sandpapers. To some extent, the excessive force to remove the sandpapers damaged the surface microstructure, which led to a decline of the water contact angle. Nevertheless, the later start of templating such as using 60 min curing PU would create a surface with high elastic deformation restorability, which resulted in a poor printing effect and a lower contact angle. The sample fabricated with the starting time of 45 min showed an obvious hydrophobic behavior with the contact angle of 102 ± 3°. Thus, the 45 min was the optimum templating starting time and would be used through the later experiments.

**Table 4** Water contact angles for the smooth PU surface and rough PU surfaces with different starting time of molding process using the 240-grit sandpaper template.

| Sample | Smooth PU | PU0 | PU15 | PU30 | PU45 | PU60 |
|---|---|---|---|---|---|---|

| | | | | | | |
|---|---|---|---|---|---|---|
| Contact angle (°) | 67 ± 2 | 79 ± 5 | 85 ± 3 | 91 ± 3 | 102± 3 | 88 ± 2 |

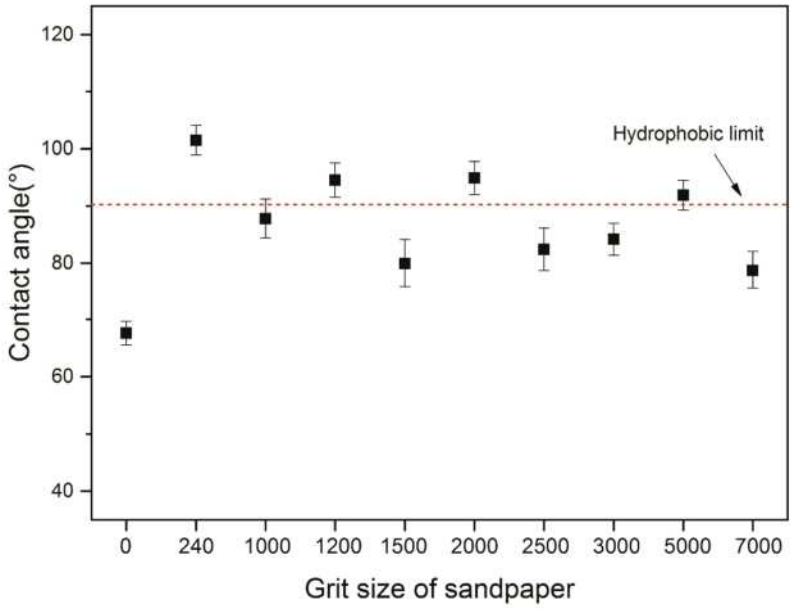


**Fig. 2.** Contact angles of PU surfaces produced using different sandpaper templates.

Fig. 2 and Table 5 illustrated the contact angle values of PU samples prepared by different types of sandpapers. PU-1, PU-3, PU-5 and PU-8 realized the transition from hydrophilic to hydrophobic states on intrinsically hydrophilic PU surfaces by building various rough microstructures. Among them, PU-1 showed the best water repelling peformance, which implied that the surface geometric structural parameters provided by the 240-grit sandpapers promoted the surface hydrophobicity more effectively.

3.2 Characterization of PU/$SiO_2$ nanocomposite surfaces

3.2.1 Enhancement in water repellency using silica nanoparticles

Nano-silica particles were used to construct nanostructures and further improve the water repellent property. To verify the effect of silica nanoparticles, PU/$SiO_2$ nanocomposites containing 4 wt% nanoparticles were prepared by the templating method using different sandpapers. The wettability of the resulting PU/$SiO_2$ nanocomposite surfaces was also traced by contact angle measurements. As

shown in Table 5, the water contact angles of the nanocomposite surfaces increased significantly, compared with those of PU surfaces without silica nanoparticles, contributed from the hydrophobic silica nanoparticles, as well as the nanostructures created on the surface.

**Table 5** Water contact angles of the PU surfaces without nanoparticles and PU/$SiO_2$ nanocomposite surfaces with different sandpaper templates.

| | Grit size of sandpaper | 0 | 240 | 1000 | 1200 | 1500 | 2000 | 2500 | 3000 | 5000 | 7000 |
|---|---|---|---|---|---|---|---|---|---|---|---|
| Contact angle (°) | PU | 67 ± 2 | 102 ± 3 | 88 ± 3 | 95 ± 3 | 80 ± 4 | 95 ± 3 | 82 ± 4 | 84 ± 3 | 92 ± 2 | 79 ± 3 |
| | PU/$SiO_2$ | 136 ± 2 | 152 ± 2 | 136 ± 3 | 141 ± 3 | 133 ± 2 | 142 ± 3 | 134 ± 2 | 135 ± 2 | 138 ± 2 | 128± 3 |

Fig. 3 depicts the influences of the silica contents in the PU/$SiO_2$ nanocomposites using 240-grit sandpaper on the contact angle values. It was discovered that nano-silica particles with content higher than 6 wt% could not fully be added to the prepared PU surfaces, so the silica content was studied from 1.5 to 6 wt%. According to Fig. 3, the composite surfaces with 1.5 to 3 wt% silica nanoparticles had the contact angles increasing from 116 ± 2° to 137 ± 3°. Although the contact angles of the nanocomposite surfaces are much larger than those of the pure PU surfaces, the experimental phenomenon showed that the water droplets were difficult to roll off from these surfaces of the composites containing 1.5 to 3 wt% silica nanoparticles and exhibited sticky behaviors. This may be because the silica content is too low to cover the entire PU surface or not enough to modify the microstructure perfectly. Interestingly, the water droplet could easily roll off from the surfaces with the higher contents of silica nanoparticles from 4 to 6 wt%, showing the desirable hydrophobic capability and the self-cleaning performance. However, the contact angle values did not keep increasing with the increase of silica concentrations. Samples with the silica nanoparticle in excess of 4 wt% (for example

PU-Si5 and PU-Si6) revealed no remarkable changes in the contact angle value, and both values were around 142°. This was because the excessive silica nanoparticles overwrote the microstructures constructed by sandpaper templates, which resulted in less decoration effect for the micro-scaled structures and influenced the formation of effective dual roughness. PU-Si4 demonstrated the highest contact angle of 152 ± 2° on the homogeneous surfaces with high hydrophobicity, while the value on the smooth PU surface with 4 wt% silica nanoparticles was 136 ± 2°. Consequently, the roughness created by both the templates and nanoparticles has significant effects on the hydrophobicity of the surfaces, which will be further investigated by SEM.

The PU/$SiO_2$ nanocomposite surface fabrication process was further optimized. Table 6 shows the effect of the molding pressure on the wettability of the PU/$SiO_2$ nanocomposite surfaces consisting of 4 wt% silica using the 240-grit sandpaper template. The contact angle firstly increased with the pressure and then decreased. According to the experimental results, the pressure of 5 MPa was the most appropriate for fabircating the highly hydrophobic surface.

**Table 6** Water contact angles for the PU/$SiO_2$ nanocomposite surfaces consisting of 4 wt% silica with different molding pressure using the 240-grit sandpaper template.

| Molding Pressure (MPa) | 3 | 4 | 5 | 6 | 8 |
|---|---|---|---|---|---|
| Contact angle (°) | 130 ± 3 | 143 ± 1 | 152 ± 2 | 145 ± 2 | 139 ± 2 |

The hydrophobic stability of the prepared surface after storing in air for various time intervals was also evaluated. The water contact angle of the PU-Si4 nanocomposite surface still remained above 150° after storing three months in air, indicating the long-term hydrophobic stability of the surface. In order to further verify the stability of the surface, the contact angles of the PU-Si4 sample were measured after 10, 30, 60 and 90 days under shear force and impact force conditions. The contact

223 angles decreased extremely slowly with the final value of 150 ± 1° and the water droplets still kept
224 rolling easily from the surface, which confirmed the stability of the PU/$SiO_2$ layer under shear force
225 and impact force conditions.

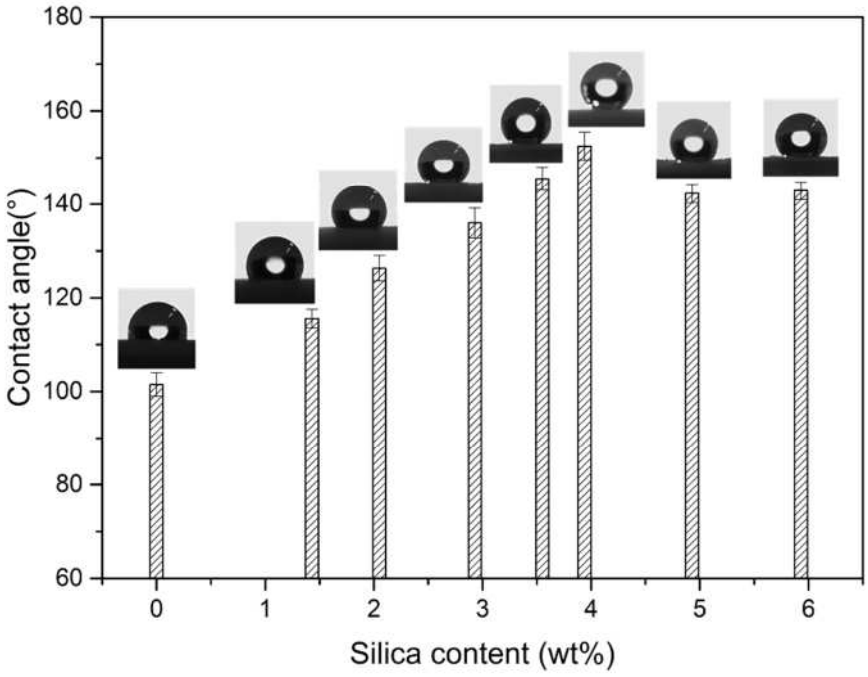


226 **Fig. 3.** Contact angles of pure PU and PU/$SiO_2$ nanocomposite surfaces consisting of different silica
227 contents with 240-grit sandpaper template.

228 3.2.2 Analysis of surface compositions

229 To investigate the influence of surface compositions on the wetting ability, the PU and PU/$SiO_2$
230 samples were studied by XPS and ATR-IR, as shown in Table 7 and Fig. 4, respectively. XPS results,
231 reported in Table 7, showed the compositions on the outer top layer of the rough surface up to 10 nm
232 in thickness direction. The very low atomic content of nitrogen confirmed the fact that there still
233 existed a little amount of PU on the outer layer of the surface, which indicated that the nano-silica
234 particles were possibly embedded into the top layer of PU. The high atomic content of silicon indicated

235 that there was a large-area coverage of silica nanoparticles on the outer layer of the nanocomposite
236 surface. ATR-IR was studied with the incident angle of 45° and the surface compositions up to 3.6 μm
237 in thickness direction were calculated according to Harrick's formula [32]. The peaks at 1259 and 799
238 $cm^{-1}$ related to the Si-C bonds and the intensive bands in the region of 1069 and 469 $cm^{-1}$ due to the
239 Si-O-Si vibration in Fig. 4b and 4c are specific to the silica nanoparticles with the modification of
240 PDMS. The broad peak at around 3274 $cm^{-1}$ and the peak at around 1727 $cm^{-1}$ are assigned to the N-
241 H stretching and C=O group in PU, respectively. These results demonstrated that both the PU and the
242 PDMS modified silica nanoparticles were present in the surface structure. An organic–inorganic hybrid
243 structure was fabricated in the upper surface of the PU/$SiO_2$ nanocomposites. It meant that some nano-
244 silica particles were partially embedded into PU during the templating and pressing process, which
245 need further determination by SEM. The intensity ratio of Si-C and C=O of the PU-Si4 sample was
246 calculated and the result was around 6:5, which represented that the average silica content in the
247 surface layer of up to 3.6 μm thickness of the PU/$SiO_2$ nanocomposites was 54.5 wt%. This value is
248 much larger than overall figure of 4 wt% in the PU/$SiO_2$ nanocomposites, which reveals that this top
249 layer of the surface mainly contained nano-silica particles. Similarly, the intensity ratio of Si-C and
250 C=O of PU-Si6 was 11:5, which meant that the silica content was 68.8 wt% in the depth from 0 to 3.6
251 μm. This confirmed that a small amount of silica addition could bring a great change on the top layer
252 of PU/$SiO_2$ nanocomposites.

253 **Table 7** XPS atomic content (at%) for PU-Si4 and PU-Si6 sample.

| Atom | C | O | Si | N |
|---|---|---|---|---|
| PU-Si4 | 50.63 | 27.48 | 21.14 | 0.74 |

| | | | | |
|---|---|---|---|---|
| PU-Si6 | 49.23 | 27.9 | 22.28 | 0.59 |

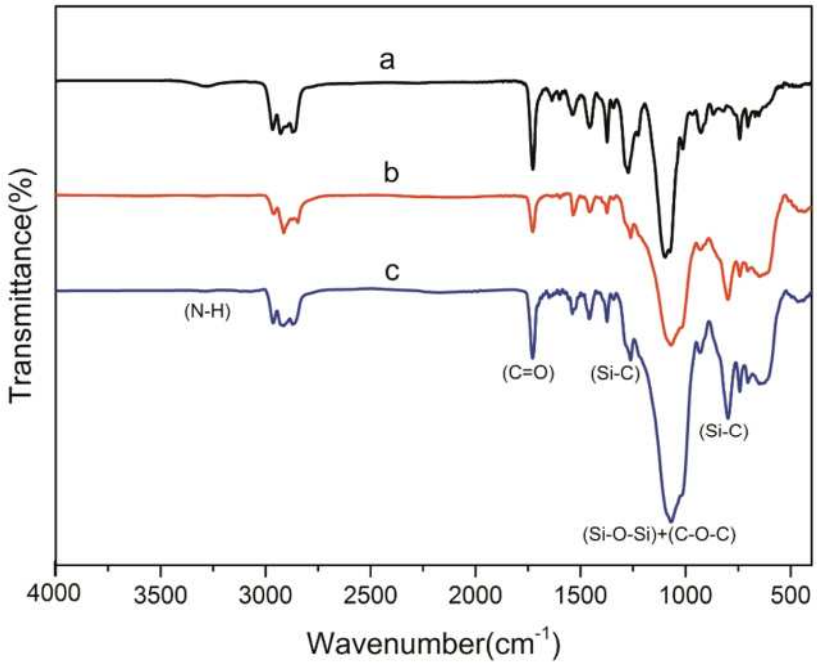


**Fig. 4.** ATR-IR spectra for PU samples containing various silica contents (a) pure PU; (b) PU-Si4; (c) PU-Si6.

3.2.3 Surface morphology and hierarchical structures

The morphology of the pure PU and PU/$SiO_2$ nanocomposite surfaces fabricated with the 240-grit template was observed by SEM, as shown in Fig. 5 and Fig. 6. It is found that PU-1 with the contact angle of 102 ± 3° exhibited a particular surface morphology with the sandpaper template in Fig. 5b. The size of the micro-scale protrusion is around 90 μm and the height is around 19 μm. As illustrated in Fig.5d, the PU-Si4 surface with the water angle of 152 ± 2° had unique micro-nano hierarchical structures. The micrograph of the cross sections of the PU-Si4 sample was also investigated by SEM. As confirmed in Fig. 6, the complex hierarchical structure is apparently formed on the PU-Si4 nanocomposite surface. Particularly, the enlarged view of a single micro protrusion in Fig. 6b reveals that on the surface of each micro protrusion, many nano papillae are distributed

randomly with diameter around 100 nm. This special structure is similar to the magnifying lotus-leaf papilla which is verified to be responsible for its excellent water repellent ability [33.34]. Besides, the cross-sectional images confirmed that the top surface was covered with large area of silica and the silica nanoparticles were partly embedded into PU, consistent with the FTIR results. On further observation, some boundaries between PU and PU silica nanoparticles are diffuse, which indicates that there was a strong interfacial bonding between the two phases. The interfacial bond directly enhanced adhesion between the particles and PU, and improved the durability of the nanocomposite surface. As demonstrated in Fig.5c, with a small amount of silica nanoparticles on the surface, the nanostructures on the PU-Si1.5 surface are difficult to be observed, which was because most of the silica nanoparticles were embedded into the PU surface. PU-Si1.5 presented some hydrophobicity with the contact angle increasing from 102 ± 3° to 118 ± 3° with 240-grit sandpaper template. Fig. 5e shows that superabundant nanoparticles (6wt% of the PU/$SiO_2$ nanocomposites) can not only fill the micro-scaled grooves but also easily lead to the agglomeration of silica nanoparticles, resulting in a damage of surface characteristics and a decrease of the water contact angle from 152 ± 2° to 142 ± 2°.

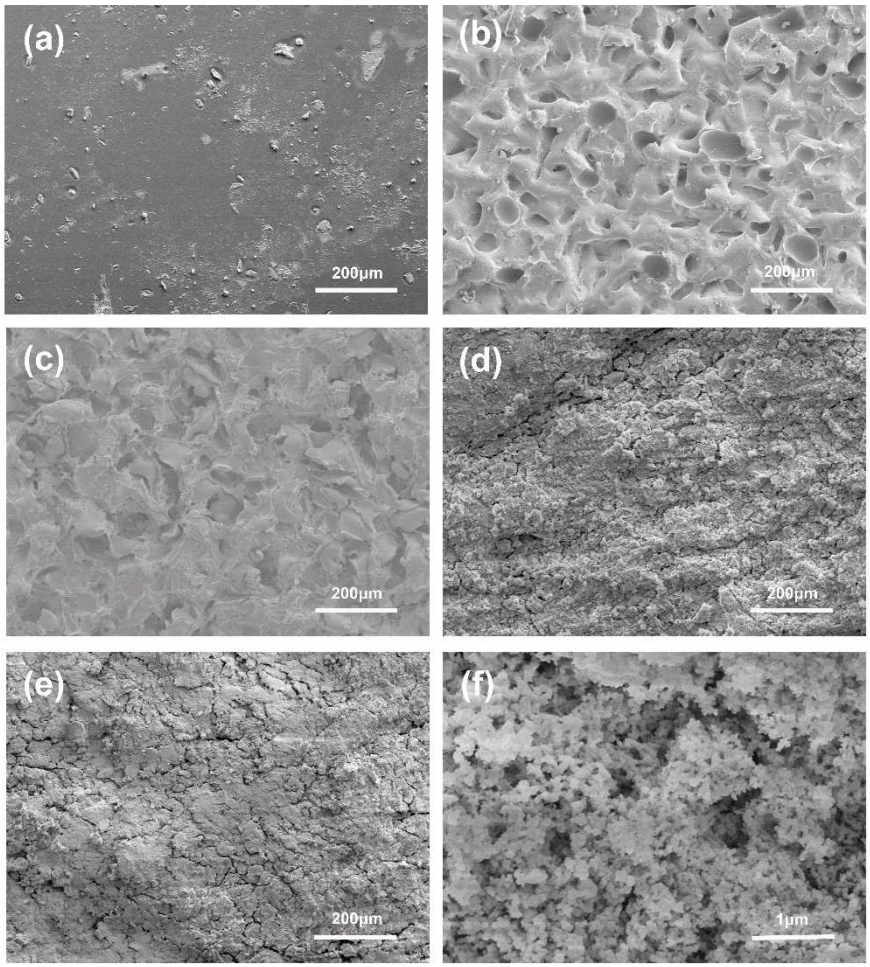


**Fig. 5.** SEM images of pristine PU and PU/$SiO_2$ nanocomposite surfaces (a) pristine PU; (b) PU-1; (c) PU-Si1.5; (d) PU-Si4; (e) PU-Si6; (f) higher magnification of (d).

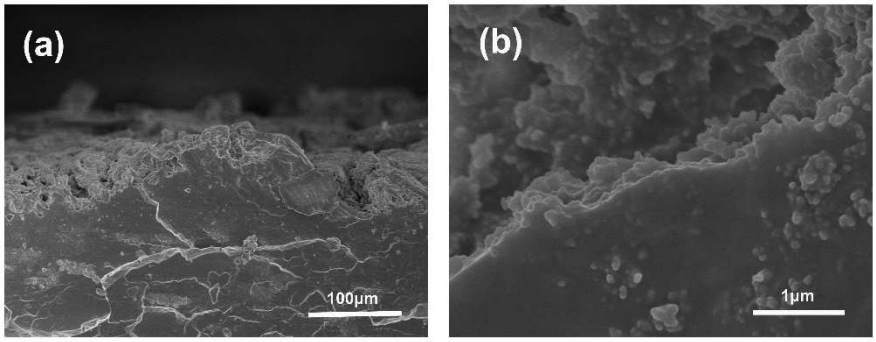


**Fig. 6.** SEM images of the cross section of PU-Si4 at different magnifications: (a) 400× and (b) 20000×.

To further analysis the mechanism of the wetting performance, two prominent models, Wenzel model [35] and Cassie-Baxter model [36], are used to explain the interaction of water droplets with a

rough surface. When the rough surface is composed of the pillars with inclined side walls, the theoretic contact angle of the hydrophobic surface in the Wenzel ($\theta_w$) and Cassie-Baxter ($\theta_{c-b}$) states are expressed as the following equations [37.38], respectively,

$$\cos\theta_w = [1 + 4(h/a)/(1 + b/a)^2]\cos\theta_e \quad (2)$$

$$\cos\theta_{c-b} = (1 + \cos\theta_e)/(1 + b/a)^2 - 1 \quad (3)$$

where $\theta_e$ is the equilibrium contact angle of the water droplet on a smooth surface. The height, the bottom side length and the distance between two pillars at the bottom are regarded as *a*, *h* and *b*, respectively. The geometric parameters of the pillars on the rough surfaces were measured by the 3D digital microscope, as shown in Fig.7.

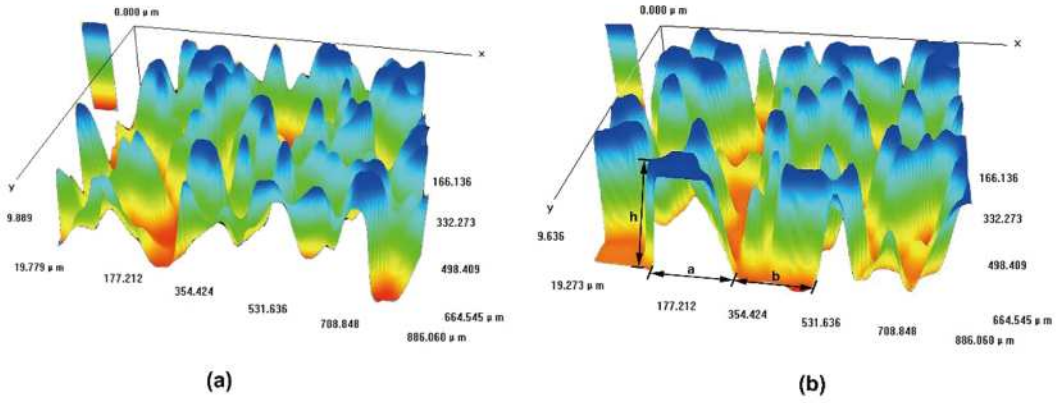


**Fig. 7.** 3D images of the surfaces of (a) PU-1 and (b) PU-Si4 sample with the 240-grit sandpaper template.

*h/a*, *b/a*, $\theta_w$ and $\theta_{c-b}$ were calculated and listed in Table **8**. The measured contact angles ($\theta_r$) of the rough pure PU-1 surfaces fabricated only by 240-grit template are between the values of $\theta_w$ and $\theta_{c-b}$. This indicated that the wetting state of the micro-scaled structures was at a transition stage between Wenzel and Cassie-Baxter states, which also showed that the water droplet wetted the microstructure at a certain extent. The contact angle of the smooth PU surface of the nanocomposite containing 4 wt% nano-silica was 136 ± 2 °, and the expected $\theta_{c-b}$ value of PU-Si4 surface was 155 °

calculated by Eq. (3), in good agreement with the experimental value of 152 ± 2 °, indicating that the nanocomposite surface followed the mechanism of Cassie-Baxter state. The nanoparticles in conjunction with the micro-scale structure of the surface formed a dual-scale rough surface and created many tiny air pockets on the top surface, which reduced the area fraction of the solid-liquid contact surface and contributed to the hydrophobicity.

On the PU-Si4 nanocomposite surface, the hydrophobic compositions provided by PDMS modified nano-silica decreased the surface energy and enlarged the intrinsic contact angle of the polymer surface. The sharp increase of the intrinsic contact angle was also the reason for the high hydrophobicity besides the geometric parameters of the rough structures. Thus, the highly hydrophobic nanocomposite surface was produced by the combination of the special hierarchical structures and the low surface energy composition.

It can be concluded that by well controlling the size of the template and the contents of nanoparticles, it is possible to adjust the geometric parameters of the micro-nano hierarchical structure and change the wettability of the surface. The result also indicates that the combined method may be applied to large-area preparation with the advantages of simplicity and flexibility.

**Table 8** Geometric parameters and contact angles of micro pillars obtained with different grit sizes of sandpapers. ($\theta_r$ is the measured value of the water contact angle.)

| Sample | Geometric parameter | | $\theta_e$ (°) | $\theta_w$ (°) | $\theta_{c-b}$ (°) | $\theta_r$ (°) |
|---|---|---|---|---|---|---|
| | h/a | b/a | | | | |
| PU-1 | 0.24 | 0.77 | 67 ± 2 | 60 | 124 | 102 ± 3 |
| PU-Si4 | 0.25 | 0.76 | 136 ± 2 | 163 | 155 | 152 ± 2 |

## 4 Conclusions

A simple and effective method to fabricate highly hydrophobic two-component TSU surfaces was developed with sandpaper templates and modified nano-silica. After cured for 45 min at the room temperature, the studied PU was subsequently covered with 240-grit sandpapers and continued to cure for another 24 h, specific micro-scale structures were formed on the surface and the water contact angle of the surface was 102 ± 3 °. According to the SEM and ATR results, the silica nanoparticles content had a significant influence on the surface morphology and compositions. The PU/$SiO_2$ nanocomposite surface with 4 wt% nano-silica particles exhibited a unique hierarchical structure consisting of micro protrusions and nano papillae. Moreover, the nanoparticles were partially embedded into the polymer during the templating and pressing process, which contributed to the adhesion and the durability of the highly hydrophobic layer. The nanocomposite surface containing 4 wt% nano-silica showed excellent water repellency with the contact angle of 152 ± 2°. The geometric parameters of the special hierarchical structures and the theoretical model explained that the cooperation of the unique micro-nano dual structure. There is a good potential to apply this simple technique to large-area fabrication in the future. The highly hydrophobic surface can be simply and large-area fabricated with good stability, which makes it possible to be applied to the self-cleaning, moisture-proof and waterproof materials.

**Conflict of interests**

This research did not receive any specific grant from funding agencies in the public, commercial, or not-for-profit sectors.

**References**

[1]H. Khatoon, S. Ahmad, A review on conducting polymer reinforced polyurethane composites, Journal of Industrial & Engineering Chemistry, (2017).

[2]R. Verdejo, R. Stämpfli, M. Alvarez-Lainez, S. Mourad, M.A. Rodriguez-Perez, P.A. Brühwiler, M. Shaffer, Enhanced acoustic damping in flexible polyurethane foams filled with carbon nanotubes, Composites Science & Technology, 69(2009) 1564-1569.

[3]G.M. Estes, R.W. Seymour, S.L. Cooper, Infrared Studies of Segmented Polyurethane Elastomers. II. Infrared Dichroism, MACROMOLECULES, 4(1971) 452-457.

[4]Q. Meng, J. Hu, Y. Zhu, J. Lu, Y. Liu, Polycaprolactone-based shape memory segmented polyurethane fiber, J. APPL POLYM SCI, 106(2010) 2515-2523.

[5]E.K. Leitsch, W.H. Heath, J.M. Torkelson, Polyurethane/polyhydroxyurethane hybrid polymers and their applications as adhesive bonding agents, International Journal of Adhesion & Adhesives, 64(2016) 1-8.

[6]T. Vélez-Pagés, J.M. Martín-Martínez, Application of one-component primer to avoid the roughening of leather and increase its adhesion to polyurethane adhesive, International Journal of Adhesion & Adhesives, 25(2005) 320-328.

[7]D.K. Chattopadhyay, K.V.S.N. Raju, Structural engineering of polyurethane coatings for high performance applications ☆, PROG POLYM SCI, 32(2007) 352-418.

[8]S. Kumari, A.K. Mishra, D.K. Chattopadhyay, K.V.S.N. Raju, Synthesis and characterization of hyperbranched polyesters and polyurethane coatings, Journal of Polymer Science Part A Polymer Chemistry, 45(2010) 2673-2688.

[9]J.P. Santerre, K. Woodhouse, G. Laroche, R.S. Labow, Understanding the biodegradation of polyurethanes: from classical implants to tissue engineering materials, BIOMATERIALS, 26(2005) 7457-7470.

[10]J. Baghdachi, H. Perez, P. Talapatcharoenkit, B. Wang, Design and development of self-stratifying

systems as sustainable coatings, PROG ORG COAT, 78(2015) 464-473.

[11]J.C. Wang, Y.H. Chen, R.J. Chen, Preparation of thermosetting polyurethane nanocomposites by montmorillonite modified with a novel intercalation agent, Journal of Polymer Science Part B Polymer Physics, 45(2010) 519-531.

[12]A. Steele, I. Bayer, E. Loth, Adhesion strength and superhydrophobicity of polyurethane/organoclay nanocomposite coatings, J. APPL POLYM SCI, 125(2012) E445-E452.

[13]A. Steele, I. Bayer, E. Loth, Adhesion strength and superhydrophobicity of polyurethane/organoclay nanocomposite coatings, J. APPL POLYM SCI, 125(2012) E445-E452.

[14]Y. Tang, J. Yang, L. Yin, B. Chen, H. Tang, C. Liu, C. Li, Fabrication of superhydrophobic polyurethane/MoS 2 nanocomposite coatings with wear-resistance, Colloids & Surfaces A Physicochemical & Engineering Aspects, 459(2014) 261-266.

[15]Z. Cheng, J. Gao, L. Jiang, Tip Geometry Controls Adhesive States of Superhydrophobic Surfaces, LANGMUIR, 26(2010) 8233-8238.

[16]W. Zhong, Y. Li, Y. Wang, X. Chen, Y. Wang, W. Yang, Superhydrophobic polyaniline hollow bars: Constructed with nanorod-arrays based on self-removing metal-monomeric template, Journal of Colloid & Interface Science, 365(2012) 28-32.

[17]J. Goscianska, A. Olejnik, R. Pietrzak, Adsorption of l -phenylalanine on ordered mesoporous carbons prepared by hard template method, J. TAIWAN INST CHEM E., 45(2014) 347-353.

[18]T. Feng, G. Zhang, Y. Wang, C. Gao, Z. Zhang, E. Xie, Photocatalytic properties of titania/porous carbon fibers composites prepared by self-template method, J. MATER SCI, 50(2015) 2921-2931.

[19]Manhui Sun, Chunxiong Luo, Luping Xu, H. Ji, Q. Ouyang, A. Dapeng Yu, Y. Chen, Artificial Lotus Leaf by Nanocasting, Langmuir the Acs Journal of Surfaces & Colloids, 21(2005) 8978.

[20]Y. Li, W. Cai, G. Duan, B. Cao, F. Sun, F. Lu, Superhydrophobicity of 2D ZnO ordered pore arrays formed by solution-dipping template method., Journal of Colloid & Interface Science, 287(2005) 634-639.

[21]X. Zhao, W. Li, Morphology and hydrophobicity of a polyurethane film molded on a porous anodic alumina template, SURF COAT TECH, 200(2006) 3492-3495.

[22]H. Ogihara, J. Xie, J. Okagaki, T. Saji, Simple method for preparing superhydrophobic paper: spray-deposited hydrophobic silica nanoparticle coatings exhibit high water-repellency and transparency., Langmuir the Acs Journal of Surfaces & Colloids, 28(2012) 4605.

[23]L. Xue, J. Li, J. Fu, Y. Han, Super-hydrophobicity of silica nanoparticles modified with vinyl groups, Colloids & Surfaces A Physicochemical & Engineering Aspects, 338(2009) 15-19.

[24]G. Leder, T. Ladwig, V. Valter, S. Frahn, J. Meyer, New effects of fumed silica in modern coatings, PROG ORG COAT, 45(2002) 139-144.

[25]Z. Wu, H. Wang, M. Xue, X. Tian, X. Ye, H. Zhou, Z. Cui, Facile preparation of superhydrophobic surfaces with enhanced releasing negative air ions by a simple spraying method, COMPOS SCI TECHNOL, 94(2014) 111-116.

[26]W.S.Y. Wong, Z.H. Stachurski, D.R. Nisbet, A. Tricoli, Ultra-Durable and Transparent Self-Cleaning Surfaces by Large-Scale Self-Assembly of Hierarchical Interpenetrated Polymer Networks, ACS APPL MATER INTER, 8(2016) 13615.

[27]J. Seyfi, S.H. Jafari, H.A. Khonakdar, G.M.M. Sadeghi, G. Zohuri, I. Hejazi, F. Simon, Fabrication of robust and thermally stable superhydrophobic nanocomposite coatings based on thermoplastic polyurethane and silica nanoparticles, APPL SURF SCI, 347(2015) 224-230.

[28]J. Seyfi, I. Hejazi, S.H. Jafari, H.A. Khonakdar, F. Simon, Enhanced hydrophobicity of

polyurethane via non-solvent induced surface aggregation of silica nanoparticles, Journal of Colloid & Interface Science, 478(2016) 117-126.

[29]F. Cirisano, A. Benedetti, L. Liggieri, F. Ravera, E. Santini, M. Ferrari, Amphiphobic coatings for antifouling in marine environment, Colloids & Surfaces A Physicochemical & Engineering Aspects, 505(2016) 158-164.

[30]M. Ferrari, A. Benedetti, E. Santini, F. Ravera, L. Liggieri, E. Guzman, F. Cirisano, Biofouling control by superhydrophobic surfaces in shallow euphotic seawater, Colloids & Surfaces A Physicochemical & Engineering Aspects, 480(2015) 369-375.

[31]A. Benedetti, F. Cirisano, M. Delucchi, M. Faimali, M. Ferrari, Potentiodynamic study of Al－Mg alloy with superhydrophobic coating in photobiologically active/not active natural seawater, Colloids & Surfaces B Biointerfaces, 137(2015) 167.

[32]N.J. Harrick, TOTAL INTERNAL REFLECTION AND ITS APPLICATION TO SURFACE STUDIES, ANN NY ACAD SCI, 101(1963) 928-959.

[33]L. Feng, S. Li, Y. Li, H. Li, L. Zhang, J. Zhai, Y. Song, B. Liu, L. Jiang, D. Zhu, Super－Hydrophobic Surfaces: From Natural to Artificial, Cheminform, 34(2002) 1857-1860.

[34]W. Barthlott, C. Neinhuis, Purity of the sacred lotus, or escape from contamination in biological surfaces, 202(1997) 1-8.

[35]R.N. Wenzel, RN, “Resistance of Solid Surfaces to Wetting by Water.” Ind. Eng. Chem., 28 988-994, Ind. Eng:chem, 28(1936) 988-994.

[36]S. Baxter, A.B.D. Cassie, 8—THE WATER REPELLENCY OF FABRICS AND A NEW WATER REPELLENCY TEST, Journal of the Textile Institute Transactions, 36(1945) T67-T90.

[37]N.A. Patankar, Transition between superhydrophobic states on rough surfaces, Langmuir the Acs

Journal of Surfaces & Colloids, 20(2004) 7097-7102.

[38]L. Zhu, Y. Feng, X. Ye, Z. Zhou, Tuning wettability and getting superhydrophobic surface by controlling surface roughness with well-designed microstructures, Sensors & Actuators A Physical, 130(2006) 595-600.

**Graphical Abstract**